Materials Science-Poland, *Vol. 26*, *No. 3*, *2008*

Synthesis, characterization, and visible-light photocatalytic activity of Fe_2O_3/SnO_2 nanocomposites

H. S. ZHUANG[1*], H. L. XIA[2], T. ZHANG[1], D. C. XIAO[1]

[1]College of Environmental Science and Engineering, Donghua University, Shanghai, 201620, P. R. China

[2]Research Institute of Quality and Technical Supervision and Inspection, Taizhou, 318000, P. R. China

A novel, visible-light-activated Fe_2O_3/SnO_2 photocatalyst was prepared by the co-precipitation method, and characterized by X-ray diffraction (XRD), transmission electron microscopy (TEM), N_2 adsorption–desorption measurement and UV-Vis diffuse reflectance spectroscopy. The phase composition, crystallite size, BET surface area and optical absorption of the sample were found to vary significantly with the calcining temperature. The photocatalytic activities of Fe_2O_3/SnO_2 photocatalysts were evaluated based on the photodegradation of acid blue 62 as a probe reaction. Experimental results indicated that the Fe_2O_3/SnO_2 photocatalyst calcined at 400 °C for 3 h (the molar ratio of Fe to Sn is 2:1) exhibited maximum photocatalytic activity due to the sample with a smaller particle size of 15 nm and a higher surface area of 28.8 $m^2 \cdot g^{-1}$. Under visible light ($\lambda > 400$ nm) irradiation, the degradation rate of acid blue 62 reached 98.0% in 60 min, which is about 3.6 times higher than that of the standard P25 photocatalyst. Additionally, the efficient electron–hole separation at the Fe_2O_3/SnO_2 photocatalyst interface may play another important role in photodegradation.

Key words: *photocatalysis; Fe_2O_3/SnO_2; acid blue 62; visible light*

1. Introduction

Semiconductor photocatalysis, as one of the advanced physicochemical processes, has been extensively studied for solving existing environmental problems such as wastewater treatment [1]. The process may proceed at ambient conditions, with the use of solar light as the energy source and atmospheric oxygen as oxidant [2]. Many organic compounds have shown to be oxidized to CO_2, water and mineral acids by this method [3]. Among various oxide semiconductor photocatalysts, TiO_2 was intensively investigated because of its biological and chemical inertness, strong oxidizing power, nontoxicity and long-term stability against photo and chemical corrosion [4, 5]. How-

*Corresponding author, e-mail: huishengzhuang@126.com

ever, there is still a problem that TiO_2 is effective only under ultraviolet irradiation ($\lambda < 380$ nm) due to its large band gap (3.2 eV) [6, 7]. Furthermore, fast recombination of photogenerated electron–hole pairs hinders the commercialization of this technology [8, 9]. Therefore, it is of great interest to separate the electron–hole pairs effectively to increase the photon efficiencies and develop new visible-light-activated photocatalysts to extend the absorption wavelength range into the visible light region. In this sense, an interesting approach to deal with the issue is carried out by a coupled semiconductor technique.

In recent works, there has been a number of studies related to the photocatalytic activity of coupled semiconductor photocatalysts, such as TiO_2/CeO_2 [10], TiO_2/WO_3 [11], TiO_2/SnO_2 [12], ZnO/SnO_2 [13]. These coupled semiconductor photocatalysts may increase the photocatalytic efficiency by increasing the charge separation and extending the photo-responding range. In addition, they also exhibit fine optical properties compared with the corresponding bulk ones due to the quantum confinement effects [14].

In this study, a novel visible-light-activated coupled Fe_2O_3/SnO_2 photocatalyst was synthesized by co-precipitation. In order to optimize the preparation for the photocatalyst, a series of Fe_2O_3/SnO_2 nanocomposites with various calcination temperatures and molar ratios of Fe to Sn were prepared, and their photocatalytic activities were evaluated using the indigoid dye, acid blue 62 (AB62), as a model organic compound. Furthermore, physical and optical properties of the Fe_2O_3/SnO_2 nanocomposites have been explored. To the best of our knowledge, the Fe_2O_3/SnO_2 photocatalyst has not been reported, and it shows significantly high photocatalytic activity in degradation aqueous AB62 solution under visible light irradiation ($\lambda > 400$ nm).

2. Experiment

Reagents. All chemicals used in this study were received from the Shanghai Chemical Reagent Factory of China and used without further purification. $NH_3 \cdot H_2O$, $SnCl_4 \cdot 5H_2O$ and $FeCl_3 \cdot 6H_2O$ were the analytical reagents. The intensity of AB62 is 200%.

Preparation of photocatalysts. Fe_2O_3/SnO_2 nanocomposite powders were prepared by co-precipitation. $SnCl_4 \cdot 5H_2O$ and $FeCl_3 \cdot 6H_2O$ were used as the starting materials, and ammonia (1:1) was used as the precipitator. $SnCl_4 \cdot 5H_2O$ and $FeCl_3 \cdot 6H_2O$ were mixed at various molar ratios and dissolved in a minimum amount of deionized water. The mixed solution was stirred at room temperature and added drop-wise with the ammonia until it transformed to precipitate completely. The precipitate was filtered and washed with deionized water until no Cl^- was found in the filtrates **(**the absence of Cl ions in the filtrate was checked using aqueous $AgNO_3$ solution**).** Then the wet powder was dried at about 100 °C in air to form the precursor of the coupled Fe_2O_3/SnO_2 photocatalyst. Finally, the precursors were calcined for 3 h at varuious temperatures in air to prepare the photocatalyst powders.

Characterization of photocatalysts. To determine the crystallite size and identity of the Fe_2O_3/SnO_2 nanocomposite powders, X-ray powder diffraction (XRD) analysis was carried out using a Rigaku D/max-2550PC diffractometer with unmonochromatized CuK_α radiation (λ = 0.15406 nm), over the 2θ collection range of 0–80°. The particle sizes and shapes of the samples were tested using a Hitachi H-800 Transmission Electron Microscone(TEM). The Brunauer–Emmett–Teller (BET) surface areas were determined using a Micromeritics ASAP 2010 N_2 adsorption apparatus. UV-Vis diffuse reflectance spectra (UV-Vis DRS) were recorded in air at room temperature in the 200–800 nm wavelength range, using a PE LAMBDA35 spectrophotometer with an integrating sphere.

Photocatalytic activity measurements. A 1000 W Xe lamp positioned over the quartz glass reactor was used as the light source and visible-light-activated photocatalytic activity of Fe_2O_3/SnO_2 photocatalyst was tested with all irradiation below 400 nm removed by using a cutoff filter. The distance between the light source and the surface of the solution was 50 cm. In all experiments, the photocatalytic reaction was kept at room temperature, which was achieved by a circulating water jacket (Pyrex).

A set of photocatalytic degradation experiments in aqueous AB62 solution was performed with the following procedure: 0.25g photocatalyst powders were added into 250 ml AB62 solution with an initial concentration of 50 $mg \cdot dm^{-3}$; prior to photoreaction, the aqueous mixture was magnetically stirred in the dark for 30 min to reach adsorption–desorption equilibrium; then the reaction mixture, still stirred, was irradiated by visible light vertically from the top; during the photoreaction, the samples were drawn from the reaction suspension at 10 min time intervals; the collected samples were centrifuged at 10 000 rpm for 10 min, and then filtered through a 0.2 μm millipore filter to remove the particles; The AB62 concentrations of the filtrates were analyzed by UV-Vis spectroscopy (TU-1810) at its maximum absorption wavelength of 595 nm.

3. Results and discussion

3.1. Catalyst characterization

The XRD patterns of the Fe_2O_3/SnO_2 photocatalyst calcined at various temperatures for 3 h are shown in Fig. 1. It can be seen that the XRD pattern of the sample calcined at 300 °C (Fig. 1a) only contains broad reflections of SnO_2 indicating poorly crystallized material. While calcined at 400 °C, the diffraction peaks clearly show that the SnO_2 and Fe_2O_3 nanocrystals co-existed in the samples. With the increase of calcining temperature (at 500 °C), the phase composition is still a mixture of SnO_2 and Fe_2O_3 phases but the diffraction peak intensity obviously increases due to the growth of crystallites and enhancement of crystallization. The average grain size estimated

from the highest intensity diffraction peaks of SnO_2 (2Θ = 33.92) using Scherrer's equation were 6.8 nm, 15.0 nm and 23.7 nm for samples a, b and c, respectively. It is obvious that the crystal sizes of the samples improved with the increase of calcining temperature, while the BET surface areas decreased. These processes are summarized in Table 1.

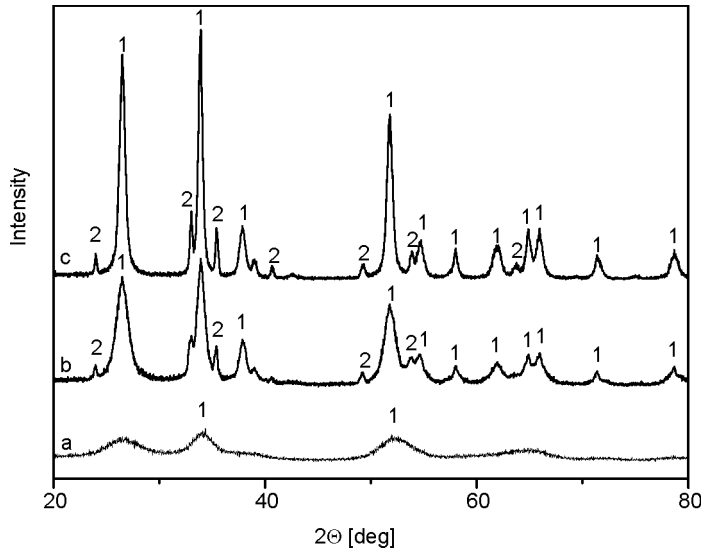

Fig. 1. XRD patterns of the Fe_2O_3/SnO_2 photocatalysts calcined at: a) 300 °C, b) 400 °C, c) 500 °C; 1 – SnO_2, 2 – Fe_2O_3

Table 1. Effect of calcination temperature on the average crystallite size and the BET surface area of the Fe_2O_3/SnO_2 samples

Calcination temperature [°C]	BET surface area[a] [$m^2 \cdot g^{-1}$]	Crystallite size[b] [nm]
300	–	6.8
350	37.4	–
400	28.8	15.0
500	16.0	23.7
600	5.6	36.2

[a]Surface area of the composite Fe_2O_3/SnO_2 photocatalyst powder.
[b]Average crystallite size calculated by applying the Scherrer formula to the highest intensity diffraction peaks of SnO_2(2Θ = 33.92).

The grain size of the Fe_2O_3/SnO_2 nanocomposite varied with calcining temperature, which has been confirmed in the TEM patterns (as shown in Fig. 2). It can be seen that the sample calcined at 300 °C appeared amorphous because of its weak crystallization. The grain edge of the sample was slightly dim (Fig. 2a). The TEM images also indicated that the grain size was homogenous and fairly small (about 15 nm)

when the sample was calcined at 400 °C. By contrast, the sample calcined at 500 °C displayed greater particle size, which is estimated to be about 25 nm due to the enhancement of crystallization or sintering between smaller particles. An increase in the calcining temperature caused the Fe_2O_3/SnO_2 photocatalyst particles to become larger. The result was in agreement with that of XRD.

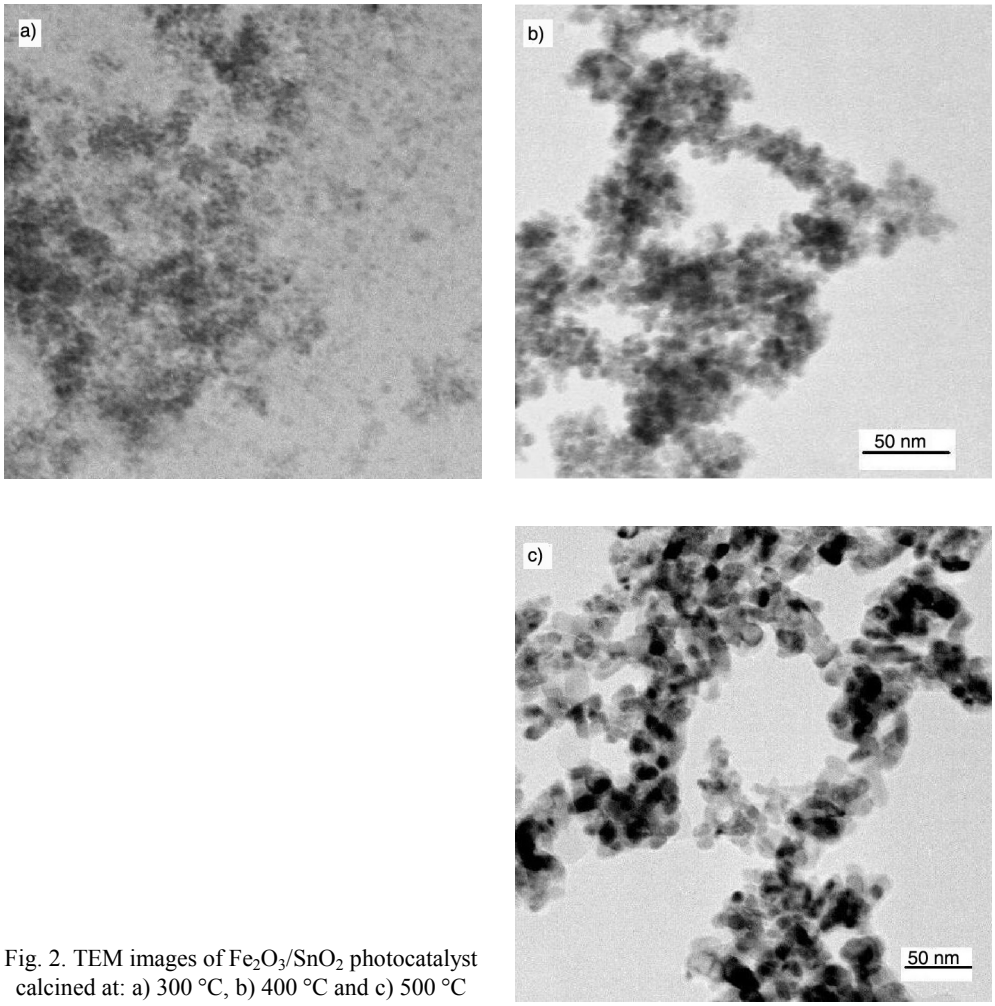

Fig. 2. TEM images of Fe_2O_3/SnO_2 photocatalyst calcined at: a) 300 °C, b) 400 °C and c) 500 °C

Figure 3 gives the UV-Vis-DRS of the Fe_2O_3/SnO_2 photocatalysts calcined at 300, 400 and 500 °C, respectively. It can be seen clearly that the intensity of reflectance is reduced with the increase of calcination temperature. This implies that the absorption edges of the samples shift to the longer wavelength range [15]. The wavelengths of absorption edges were determined by extrapolating the horizontal and sharply rising portions of the curve and defining the edge as the wavelength of the intersection [16]. When calcined at 300 °C, the sample has a little absorption in the range of visible light

and the absorption edge is about 460 nm. With the increase of calcining temperature (reached 400 °C), the absorption edge of the sample has a red-shift of about 20 nm.

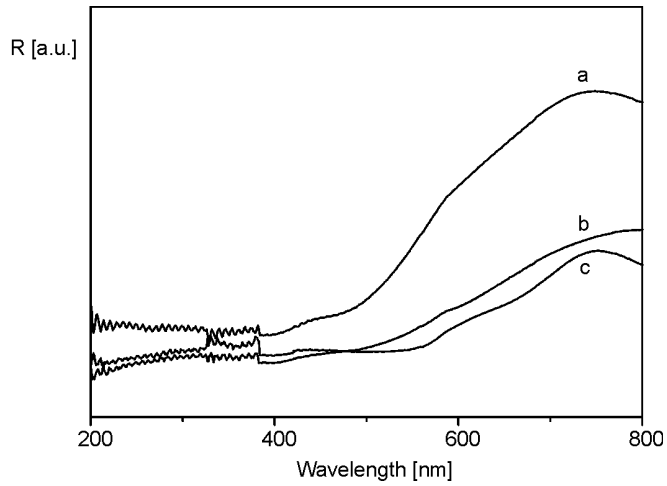

Fig. 3. UV-Vis-DRS of the Fe_2O_3/SnO_2 photocatalys calcined at: a) 300 °C, b) 400 °C and c) 500 °C

The red shift is presumably ascribed to the formation of the fairly homogenous Fe_2O_3 nanocrystals. The bandgap energy of Fe_2O_3 is 2.2 eV and it can be activated by the light below 563 nm [17], when it couples with SnO_2 semiconductor, the conduction band of SnO_2 acts as a sink for photogenerated electrons. The photogenerated holes move in the opposite direction, accumulate in the valence band of Fe_2O_3 particles, which leads to an increase in charge separation efficiency and extends the photo-responding range to visible light.

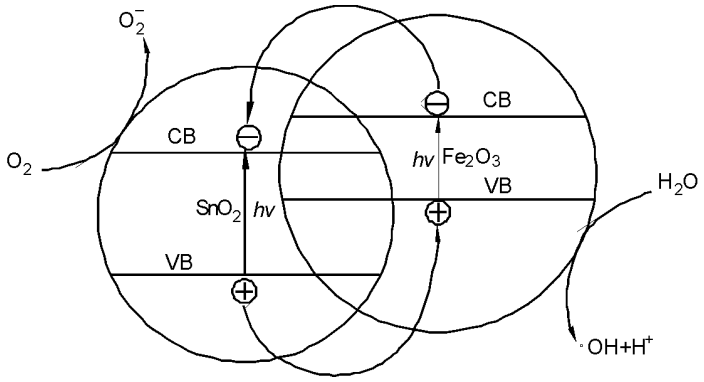

Fig. 4. Sketch map of photocatalytic mechanism of the coupled Fe_2O_3/SnO_2

The sketch map of photocatalytic mechanism of the coupled Fe_2O_3/SnO_2 is shown in Fig. 4. When the calcining temperature reaches 500 °C, the crystallite size becomes

larger, the sample shows more red shift (the absorption edge is about 530 nm) which is consistent with the result obtained by Yu et al. [18].

3.2. Photocatalytic activity studies

3.2.1 Effect of the preparation condition

It is well known that calcining temperature has a significant effect on the activity of the catalysts. Figure 5 shows the dependence of visible light photocatalytic activity on calcining temperature. It is displayed that the Fe_2O_3/SnO_2 nanocomposites calcined at 300 °C, 400 °C and 500 °C for 3 h showed higher photocatalytic activity, respectively. In the range of calcining temperature, the sample calcined at 400 °C reaches the highest photocatalytic activity with AB62 solution almost completely degradation in 60 min which may be attributed to the sample with good crystallization and high surface area. However, the photocatalytic activity of the photocatalyst decreased slightly when the calcining temperature decreased from 400 °C to 200 °C due to the weak crystallization. On the other hand, the photocatalytic activity decreased significantly when the calcining temperature increased from 500 °C to 700 °C: probably because of the decrease of surface area or occurrence of some sintering, although it had better crystallinity.

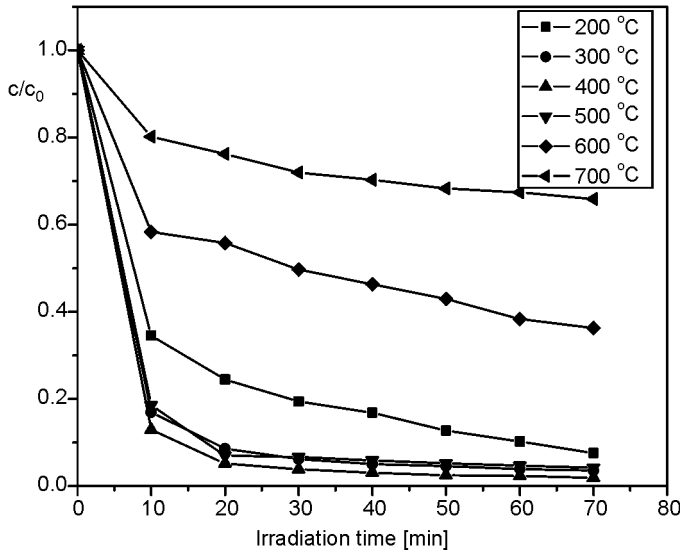

Fig. 5. Photocatalytic activity of the Fe_2O_3/SnO_2 photocatalysts calcined at various temperatures

The photocatalytic activities of the Fe_2O_3/SnO_2 nanocomposites with different molar ratios of Fe to Sn calcined at 400 °C for 3 h is shown in Fig. 6. It can be seen from Fig. 6 that pure SnO_2 showed lower photocatalytic activity compared to pure Fe_2O_3.

Therefore, the SnO_2 content should be an important factor affecting the photocatalytic activity of the Fe_2O_3/SnO_2 nanocomposite. It is obvious that the coupled Fe_2O_3/SnO_2 photocatalyst displayed higher photocatalytic activity than pure Fe_2O_3 and SnO_2, and the photocatalytic activity changed with the different molar ratio of Fe to Sn. The optimum molar ratio of Fe to Sn was 2:1, at which the photocatalytic activity of the coupled Fe_2O_3/SnO_2 photocatalyst was about 1.6 times that of the Fe_2O_3, and 5.5 times that of the SnO_2. The enhancement in the photocatalytic activity may be explained in terms of synergetic effect on the specific adsorption property and efficient electron–hole separation at the Fe_2O_3/SnO_2 interface.

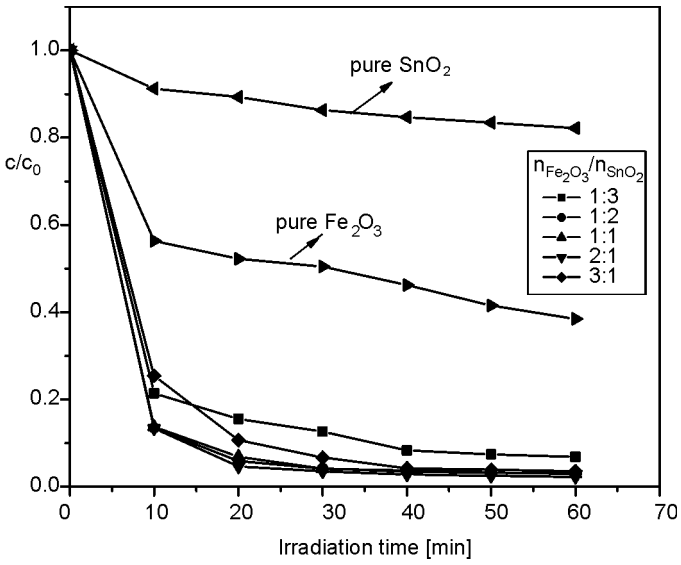

Fig. 6. Photocatalytic activity of the Fe_2O_3/SnO_2 photocatalyst with various molar ratios of Fe to Sn

Further increase in the SnO_2 or Fe_2O_3 content led to a decrease in the photocatalytic activity of the coupled Fe_2O_3/SnO_2 photocatalyst because of the lower photocatalytic activity of SnO_2 or the weaker crystallization of Fe_2O_3 at the same conditions. Therefore, for the Fe_2O_3/SnO_2 photocatalyst, the optimum photocatalytic activity in the range of our experiments appeared when the molar ratio of Fe to Sn is 2:1. A detailed theoretical explanation is in progress.

3.2.2. Comparison of photocatalytic performance

In order to explore the photocatalytic activity and stability of the Fe_2O_3/SnO_2 photocatalyst calcined at 400 °C for 3 h (the molar ratio of Fe to Sn being 2:1) under visible light ($\lambda > 400$ nm), the photocatalytic behaviour of the standard photocatalyst Degussa P25 was also measured as a reference. The result is shown in Fig. 7. The AB62 removal on the Fe_2O_3/SnO_2 photocatalyst reaches 98.0% in 60 min, obviously

higher about 3.6 times than the value of 27.4% over Degussa P25. The enhancement may be explained in terms of the synergetic effect on the specific adsorption property and efficient electron–hole separation at the Fe_2O_3/SnO_2 nanocomposites catalyst interfaces**.**

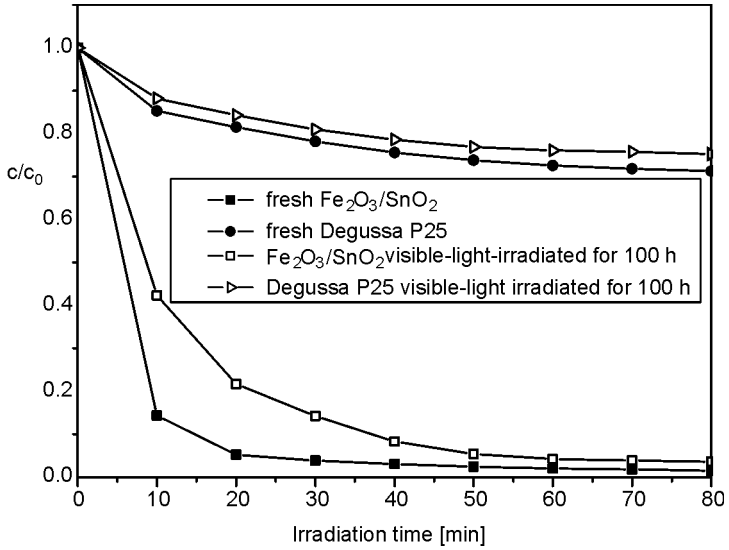

Fig. 7. Comparison for the photocatalytic activity and stability of the Fe_2O_3/SnO_2 photocatalyst with P25

It also can be seen from Fig. 7 that the photocatalytic activities became lower after the photocatalysts are irradiated for 100 h under visible light, and the long term stability of the Fe_2O_3/SnO_2 photocatalyst is poorer than that of P25. The XRD analysis indicates no changes in the phase composition of the photocatalyst after 100 h visible-light-irradiation (not shown). But the XRD results cannot rule out the possibility of the formations of some amorphous products, such as amorphous $Fe(OH)_3$, $SnO_2{\cdot}nH_2O$, Fe and Sn with no photocatalytic activity under the visible-light irradiation. It is possible that these amorphous products formed under the visible-light irradiation, which led to the decrease in the photocatalytic activity. A further study on the mechanism of deactivation is needed on this issue.

4. Conclusion

The visible-light-activated coupled Fe_2O_3/SnO_2 photocatalysts were prepared by co-precipitation. The characteristic patterns of XRD, BET, TEM and UV-Vis diffuse reflectance displayed that the sample calcined at 400 °C for 3 h (the molar ratio of Fe to Sn equal to 2:1) has better crystallinity, smaller crystal sizes and stronger response to visible light. The photocatalyst showed remarkable photocatalytic activity under

visible light ($\lambda > 400$ nm), 98.0% AB62 can be degraded in 60 min. A study on how to keep high photocatalytic activity and long term stability after many cycles of using the Fe_2O_3/SnO_2 photocatalyst is in progress. In a sense, the effective photodegradation of the dye by Fe_2O_3/SnO_2 photocatalyst under visible light is a very exciting research topic in photocatalytic area, and this work may provide new insights into the development of novel sunlight photocatalysts.

Acknowledgements

This work was supported by the National Natural Science Foundation of China (20677008) and the Innovation Foundation of Donghua University for Ph D candidates.

References

[1] RODRIGUEZ M., SARRIA V., ESPLUGAS S., PULGARIN C., J. Photochem. Photobiol. A: Chem., 151 (2002), 129.
[2] STYLIDI M., KONDARIDES D.I., VERYKIOS X.E., Appl. Catal. B: Environ., 47 (2004), 189.
[3] COLÓN G., HIDALGO M.C., NAVÍO J.A., Appl. Catal. A: Gen., 231 (2002), 185.
[4] KOSOWSKA B., MOZIA S., MORAWSKI A.W., GRZMIL B., JANUS M., Sol. Energy Mater. Sol. Cells., 88 (2005), 269.
[5] KOHTANI S., TOMOHIRO M., TOKUMURA K., NAKAGAKI R., Appl. Catal. B: Environ., 58 (2005), 265.
[6] HONG X.T., WANG Z.P., CAI W.M., LU F., ZHANG J., YANG Y.Z., MA N., LIU Y.J., Chem. Mater., 17 (2005), 1548.
[7] KUMAR S., FEDOROV A.G., GOLE J.L., Appl. Catal. B: Environ., 57 (2005), 93.
[8] YU J.G., YU J.C., CHENG B., HARK S.K., IU K., J. Solid State Chem., 174 (2003), 372.
[9] WANG C., ZHAO J.C., WANG X.M., MAI B.X., SHENG G.Y., PENG P.A., FU J.M., Appl. Catal. B: Environ., 39 (2002), 269.
[10] LIU B.S., ZHAO X.J., ZHANG N.Z., ZHAO Q.N., HE X., FENG J.Y., Surface Sci., 595 (2005), 203.
[11] TENNAKONE K., BANDARA J., Appl. Catal. A: Gen., 208 (2001), 335.
[12] LI X.Z., LI F.B., YANG C.L., GE W.K., J. Photochem. Photobiol. A: Chem., 141 (2001), 209.
[13] WANG C., WANG X.M., MAI B.X., ZHAO J.C., MAI B.X., PENG P.A., SHENG G.Y., FU J.M., J. Photochem. Photobiol. A: Chem., 168 (2004), 47.
[14] YU X.D., WU Q.Y., JIANG S.C., GUO Y.H., Mater. Charact., 57 (2006), 333.
[15] JANUS M., INAGAKI M., TRYBA B., MORAWSKI A.W., Appl. Catal. B: Environ., 63 (2006), 272.
[16] PROVENZANO P.L., JINDAL G.R., SWEET J.R., WHITE W.B., J. Lumin., 92 (2001) 297.
[17] KARUNAKARAN C., SENTHILVELAN S., Electrochem. Commun., 8 (2006), 95.
[18] YU J.G., XIONG J.F., CHENG B., YU Y., WANG J.B., J. Solid State Chem., 178 (2005), 1968.

Received 6 May 2007
Revised 4 March 2008